Tunable Electronic and Thermoelectric Performance in Twisted Bilayer Blue-Phosphorene Nanoribbon-Based Heterojunctions

Liang Zhang(张良)[1], Shihua Tan(谭仕华)[1], Xiaofang Peng(彭小芳)[1*], and Mengqiu Long(龙孟秋)[2*]

[1]*Hunan Province Key Laboratory of Materials Surface & Interface Science and Technology, Central South University of Forestry and Technology, Changsha 410004, China*
[2]*School of Physics and Electronics, Central South University, Changsha 410083, China*

(Received 1 March 2025; accepted manuscript online 23 April 2025)

In two-dimensional bilayer systems, twist-angle-dependent electronic and thermoelectric properties have garnered significant scientific interest in recent years. In this work, based on a combination of density functional theory and nonequilibrium Green's function method, we explore the electronic and thermoelectric properties in blue-phosphorene nanoribbon-based heterojunction (BPNRHJ) with and without blue-phosphorene nanoribbon (BPNR) stack. Our calculations find that the electronic conductance and power factor can be strongly enhanced by the BPNR stack, and their enhancements can be further observed with the twist between the layers. The main reason for this is the electronic hybridization between the layers can provide new transport channels, and the twist can modulate the strength of interlayer electronic hybridization, resulting in extremely violent fluctuations in electron transmission and hence an enhanced power factor. While the phonon thermal conductance exhibits very low dependence on the layer stack and twist. Combining these factors, our results reveal that the thermoelectric performance can be greatly modulated and enhanced in twist bilayer BPNRHJ: the figure of merit will be over 2.5 in 4-4-ZBPNR@ZGNR-AA-8.8° at 500 K.

DOI: 10.1088/0256-307X/42/6/066601 CSTR: 32039.14.0256-307X.42.6.066601

1. Introduction. Twist thermoelectricity, the study of how rotational mismatch between the vertically stacked layers modulates the conversion of heat flow to electrical work and *vice versa* at the nanoscale, offers new possibilities for designing novel high-performance thermoelectric devices. For coupled double-layer systems, there are various interlayer interactions, such as Coulomb exchange interaction,[1] electron–phonon interaction,[2] electron–phason interaction,[3,4] and exciton effect.[5,6] While twisting between the layers can miraculously regulate these interactions, it not only leads to novel electron and phonon properties,[7] such as flat electronic band structure,[8] Mott insulating phase,[9] unconventional superconductivity,[10] quantized anomalous Hall effect,[11] van Hove singularities,[12] chiral phonons,[13,14] and phonon-drag effect,[15,16] but also suppresses phonon transport properties, significantly improving thermoelectric performance.[17]

Based on the great advances in manufacturing technology,[18,19] quasi-one-dimensional nanoribbons can be precisely patterned from single-layer or few-layer two-dimensional materials.[20–23] Benefiting from the novel quantum confinement and edge effects, the quasi-one-dimensional nanoribbons can achieve precise control over their band structure[24] and phonon dispersion.[25] Using these individual nanoribbons as building blocks can construct various quantum geometries; the transport properties of electrons[26] and phonons[27–29] can be precisely controlled by the quantum geometries, which provides new strategies to build high-performance thermoelectric devices via device engineering.[30] Especially, owing to the independent rotational degrees of freedom in twisted bilayer nanoribbons, it has been proved both in theory[6] and experiment[16,31] that the twist angle can precisely regulate the interlayer interaction, resulting in novel electronic,[32] thermal,[33,34] and thermoelectric properties.[35]

Phosphorene, a new layered material, exhibits an anisotropic structure, a non-zero bandgap, and a relatively large mean free path, resulting in great potential in optoelectronics, electronics, and thermoelectric applications.[38] As one of the different stable structures of phosphorene,[39,40] blue phosphorene (BP), a monolayer of phosphorus atoms with a buckled honeycomb structure, has been synthesized via the epitaxial growth method.[41] Compared with another allotrope, black phosphorene, BP has only a few meV higher cohesive energy,[42] lower lattice thermal conductivity,[43] and a much higher room temperature thermoelectric figure of merit (ZT).[44] Furthermore, the black phosphorus/blue phosphorus van der Waals heterostructure[45] and foreign atom-doped BP can dramatically modulate the optical absorption,[46] magnetic,[47] and thermoelectric properties.[48,49]

In recent years, phosphorene nanoribbons have also been intensively investigated, including electronic and thermal transport properties, as well as thermoelectric en-

*Corresponding author. Email: xiaofangpeng@csuft.edu.cn; mqlong@csu.edu.cn
© 2025 Chinese Physical Society and IOP Publishing Ltd. All rights, including for text and data mining, AI training, and similar technologies, are reserved.

ergy conversion. Many interesting thermoelectric properties are found in these systems. For example, Sodagar *et al.* studied the effect of strain on the thermoelectricity and found that there is a twofold increase in the thermoelectric ZT.[50] Applying an electric field to phosphorene nanoribbons, a recent study found the even and odd effects on the thermoelectric properties.[51] More recently, Pishevar[38] and Rezayi *et al.*[52] suggested that line edge roughness and the periodic structure of vacancies can both optimize the thermoelectric performance. However, to the best of our knowledge, little attention has been paid to the twist-angle-dependent thermoelectric properties of twisted blue-phosphorene-nanoribbon (BPNR)-based heterojunction (BPNRHJ).

Twist bilayer nanoribbon-based heterojunctions could open the opportunity to create novel quantum layered stacking thermoelectric devices with tunable electronic and thermoelectric properties. In this work, we use a combination of density functional theory and the nonequilibrium Green's function method to investigate the electronic and thermoelectric properties of BPNRHJ with and without BPNR stacking. The results show that the BPNR stacking in BPNRHJ can strongly enhance the $ZT_{\max}$. This is because the stacked BPNR can provide new transport channels, which are mainly responsible for the improvement of the $ZT_{\max}$. Most importantly, the twist between the layers can modulate the strength of the interlayer electronic hybridization and further enhances the $ZT_{\max}$, which confirms that the twisted BPNRHJ can realize enhancements in thermoelectric performance.

2. Computational Methods. In the present work, the geometry of BPNRHJ is depicted in Fig. 1. The structure of the central scattering region is composed of a twisted bilayer zigzag BPNR (ZBPNR), and the stack between the layers displays two kinds of stacking configurations, namely, AA-stack and AB-stack configurations.[35] In the AA-stack configuration, the center position of the top layer ZBPNR is used as the rotation center, which maintains the rotational symmetry of the structure. In the AB-stack configuration, the top atom on the far left is used as the rotation center, which completely disrupts the rotational symmetry. The twist angle between the two single layers is θ. The 'tear-and-stack' technique[36] and atomic force microscope tip manipulation[37] can accurately control the interlayer twist, which provides the possibility for our structural reality construction.

It is noted that here the number of phosphorus dimer lines across the ribbon width is always 2, and the bottom ZBPNR plane is coplanar to ZGNR electrodes (the number of carbon dimer lines across the ribbon width is always 6). These two different types of configurations are named M-N-ZBPNR@ZGNR-AA-θ and M-N-ZBPNR@ZGNR-AB-θ (M and N represent the numbers of longitudinal repeating units of the upper and lower layer ZBPNRs in the scattering region). Especially, the geometry of N-ZBPNR@ZGNR presents a coupling configuration between

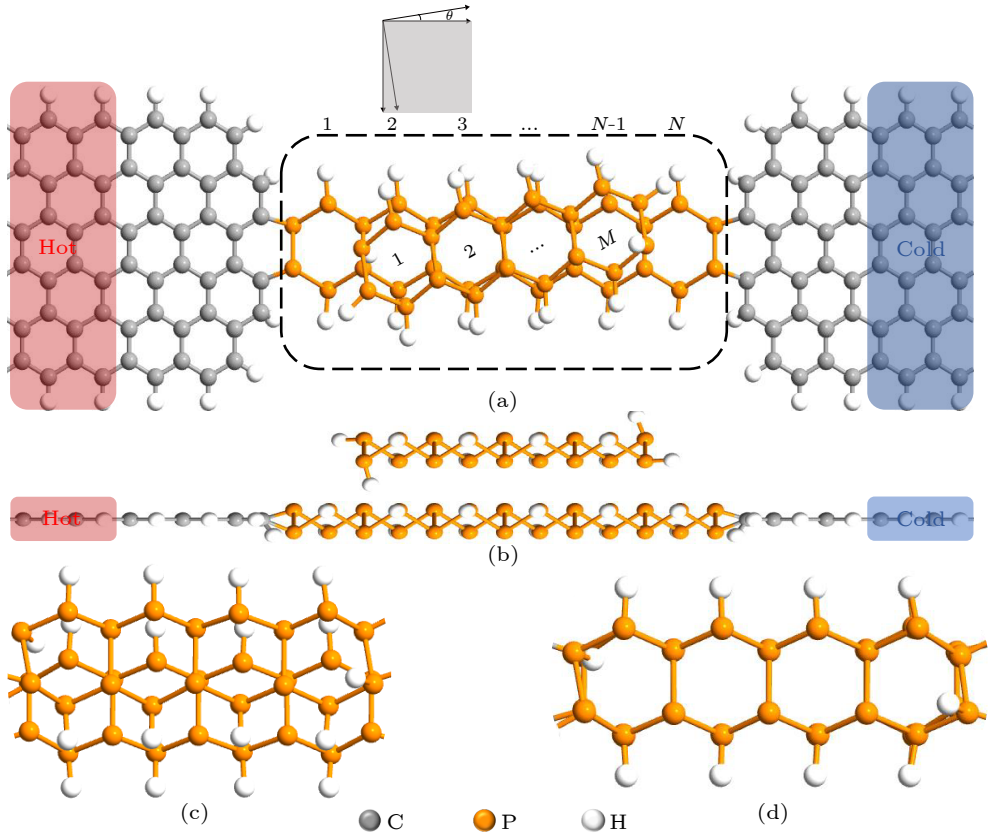

Fig. 1. Geometrical model that demonstrates M-N-ZBPNR@ZGNR-θ configuration. (a) The vertical view of M-N-ZBPNR@ZGNR-θ. (b) The side view of M-N-ZBPNR@ZGNR-θ. (c) The AB-stack. (d) The AA-stack.

the bottom layer ZBPNR and ZGNR, and the top layer ZBPNR does not exist in this geometry. Herein, all calculations are performed using density-functional theory combined with the Keldysh nonequilibrium Green's technique, which is implemented in the ATOMISTIX TOOLKIT package (ATK).[53,54] For the exchange-correlation energy function, the Perdew-Burke-Ernzerhof (PBE) version of the generalized gradient approximation (GGA) is adopted, and the DFT-D2 method of Grimme is used to modify the Van der Waals interactions.[55] The energy cutoff of real-space mesh size is set to 75 Ry, and a Monkhorst-Pack $1 \times 1 \times 25$ k-point grid is used to sample the Brillouin zone. The convergence criterions for energy and force are smaller than 10^{-5} eV and 0.05 eV/Å, respectively. A supercell with a vacuum of more than 20 Å is added to prevent interaction between adjacent images.

Once the electron and phonon transmission function $\tau_{\rm e}(E)$ and $\tau(\omega)$ are obtained, the electron conductance, electron thermal conductance, Seebeck coefficient, phonon thermal conductance,[56] and ZT[30] can be obtained from the following equations:

$$G(\mu,T) = e^2 \Gamma^{(0)}(\mu,T), \tag{1}$$

$$K_{\rm e}(\mu,T) = \frac{1}{T}\Big\{\Gamma^{(2)}(\mu,T) - \frac{[\Gamma^{(1)}(\mu,T)]^2}{\Gamma^{(0)}(\mu,T)}\Big\}, \tag{2}$$

$$S(\mu,T) = \frac{1}{eT}\frac{\Gamma^{(1)}(\mu,T)}{\Gamma^{(0)}(\mu,T)}, \tag{3}$$

$$K_{\rm ph} = \frac{\hbar^2}{k_{\rm B}T^2}\frac{1}{2\pi}\int_0^\infty \tau(\omega)\frac{\omega^2 {\rm e}^{\beta\hbar\omega}}{({\rm e}^{\beta\hbar\omega}-1)^2}{\rm d}\omega, \tag{4}$$

$$ZT = \frac{TGS^2}{K_{\rm e}+K_{\rm ph}}. \tag{5}$$

The Onsager coefficient $\Gamma^{(m)}$ is an intermediate function defined as[57]

$$\Gamma^{(m)} = \frac{2}{h}\int_{-\infty}^{\infty}(E-\mu)^m\Big[-\frac{\partial f(E,\mu,T)}{\partial E}\Big]\tau_{\rm e}(E){\rm d}E, \tag{6}$$

where $f(E,\mu,T)$ is the Fermi-Dirac distribution function at temperature T and chemical potential μ (h is the Plank constant, and E is the energy of electron). With the breakthrough of experimental technologies recently, such as atomic force microscopy,[58] AC lock-in, Raman thermometry,[59] and thermoreflectance techniques,[60] ZT also can be measured accurately.

3. Results and Discussion. To assess the dependence of the thermoelectric performance on AA and AB stackings with different twist angles, we present the thermoelectric ZT of M-N-ZBPNR@ZGNR-AA-θ and M-N-ZBPNR@ZGNR-AB-θ with different θ in Fig. 2. Moreover, the thermoelectric ZT of 4-ZBPNR@ZGNR is also presented for comparison in Fig. 2(a). It can be seen from Fig. 2(a) that the $ZT_{\rm max}$ can reach 1.9 at $\mu = -1.3$ eV in 4-ZBPNR@ZGNR without BPNR stack, which is much larger than that in blue phosphorene.[61] Obviously, the $ZT_{\rm max}$ can be improved to 2.4 at $\mu = -1.4$ eV in 2-4-ZBPNR@ZGNR-0° with BPNR stack, which is similar to the previous result, namely, these single-molecule junction and nanoribbon-based heterojunctions can significantly improve the thermoelectric ZT. However, the thermoelectric performance in these structures has a common drawback, that is, the ZT value near the Fermi level (FL) tends to approach zero.[33,55,62–64] Here, the thermoelectric performance in 4-ZBPNR@ZGNR also has a similar drawback. However, it is interesting to find that wide ZT

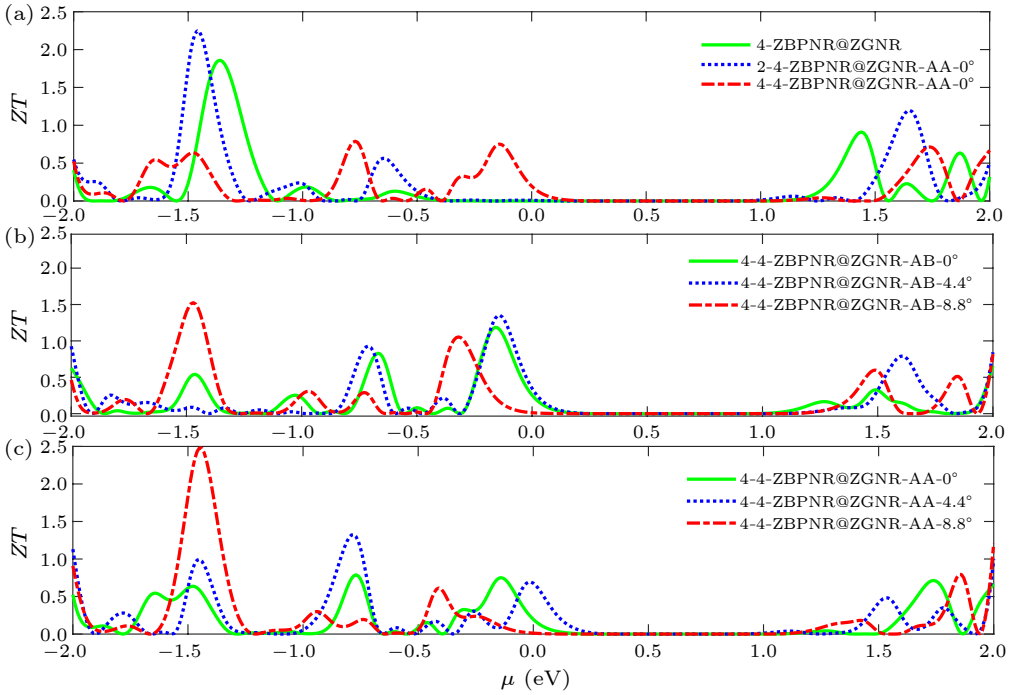

Fig. 2. The figure of merit ZT as a function of electrochemical potential μ at temperature $T = 500$ K for different configurations. (a) 4-ZBPNR@ZGNR, 2-4-ZBPNR@ZGNR-AA-0°, and 4-4-ZBPNR@ZGNR-AA-0°. (b) 4-4-ZBPNR@ZGNR-AB-0°, 4-4-ZBPNR@ZGNR-AB-4.4°, and 4-4-ZBPNR@ZGNR-AB-8.8°. (c) 4-4-ZBPNR@ZGNR-AA-0°, 4-4-ZBPNR@ZGNR-AA-4.4°, and 4-4-ZBPNR@ZGNR-AA-8.8°.

peaks appear in the structures 4-4-ZBPNR@ZGNR-AA-0° and 4-4-ZBPNR@ZGNR-AB-0° near the FL, and the $ZT_{\max}$ can even reach 1.4 in 4-4-ZBPNR@ZGNR-AB-0°, which means that layer stacking can help overcome this drawback. Furthermore, it can be seen from Figs. 2(b) and 2(c) that the chemical potential position of $ZT_{\max}$ can be modulated significantly by varying the twist angle in 4-4-ZBPNR@ZGNR-AA-θ and 4-4-ZBPNR@ZGNR-AB-θ. In addition, when the θ increases from 4.4° to 8.8°, the increased twist angle significantly improves the $ZT_{\max}$ value to 2.5 near $\mu = -1.4$ eV in 4-4-ZBPNR@ZGNR-AA-8.8°, and the corresponding $ZT_{\max}$ in 4-4-ZBPNR@ZGNR-AA-8.8° is almost three times larger than that in 4-4-ZBPNR@ZGNR-AA-4.4°. These results indicate that the twist angle is a useful degree of freedom to control the thermoelectric performance, which can not only improve ZT and tune the position of ZT near the FL, but also efficiently enhance the optimal $ZT_{\max}$.

To understand the dependence of thermoelectric properties on the stack and twist, we display the electrical transmission spectra and conductance of M-N-ZBPNR@ZGNR-AA-θ and M-N-ZBPNR@ZGNR-AB-θ with different θ in Fig. 3. Many researches showed that the destructive quantum interference can induce a very low electrical conductance, which typically occurs in some molecular rings near the FL such as 1,4-diazabicyclo[2.2.2]octane[65] and silicon-based molecules with a functionalized bicyclo[2.2.2] octasilane moiety.[66] Moreover, the interlayer coherent electronic states in bilayers exhibit a unique dependence on the twist angle, resulting in cross-plane thermoelectricity at low angles being highly sensitive to the twist.[16] Here, our calculations show that interlayer coherent electronic states are also highly sensitive to the twist angle, which can modulate the destructive quantum interference in-plane and presents some impressive transport properties. The first impressive property is that the interlayer couplings can induce conductance switching, differing from monolayer counterparts. For example, the transmission coefficient is enhanced in 4-4-ZBPNR@ZGNR-AA-0° and 4-4-ZBPNR@ZGNR-AB-0° over 4-ZBPNR@ZGNR in the energy region $-0.7\sim0$ eV. Previous studies have found that there exits strong electronic hybridization[6,16] between the layers, which may be responsible for the transmission-coefficient enhancement. To confirm this hypothesis, we plot their molecular energy spectrum (MES) in Fig. 3(d). Clearly, the layer stack can significantly increase the number of molecular energy levels (MELs), especially near the FL. These increased MELs can provide more electron transport channels, leading to larger electrical conductances of 4-4-ZBPNR@ZGNR-AA-0° and 4-4-ZBPNR@ZGNR-AB-0° near the FL. The second impressive characteristic is twist-angle-dependent thermoelectric behavior in twisted M-N-ZBPNR@ZGNR-AA-θ and M-N-ZBPNR@ZGNR-AB-θ heterostructures. It is known that the interlayer coherent electronic states are highly sensitive to the twist,[16] which will inevitably affect the electronic states and transport properties of in-plane electrons. Quantitatively, comparing the MES of 4-4-ZBPNR@ZGNR-AA-4.4° with that of 4-4-ZBPNR@ZGNR-AA-0°, the twist induces the MELs to significantly approach the FL. Thus, lower energy electrons can be transmitted from the left electrode to the right electrode, resulting in some transmission peaks and thus increased electrical conductance peaks further close to the FL. However, for the 4-4-ZBPNR@ZGNR-AB-θ heterostructure, the MELs near the FL present an opposite trend when the twist angle increases from 4.4° to 8.8°. As

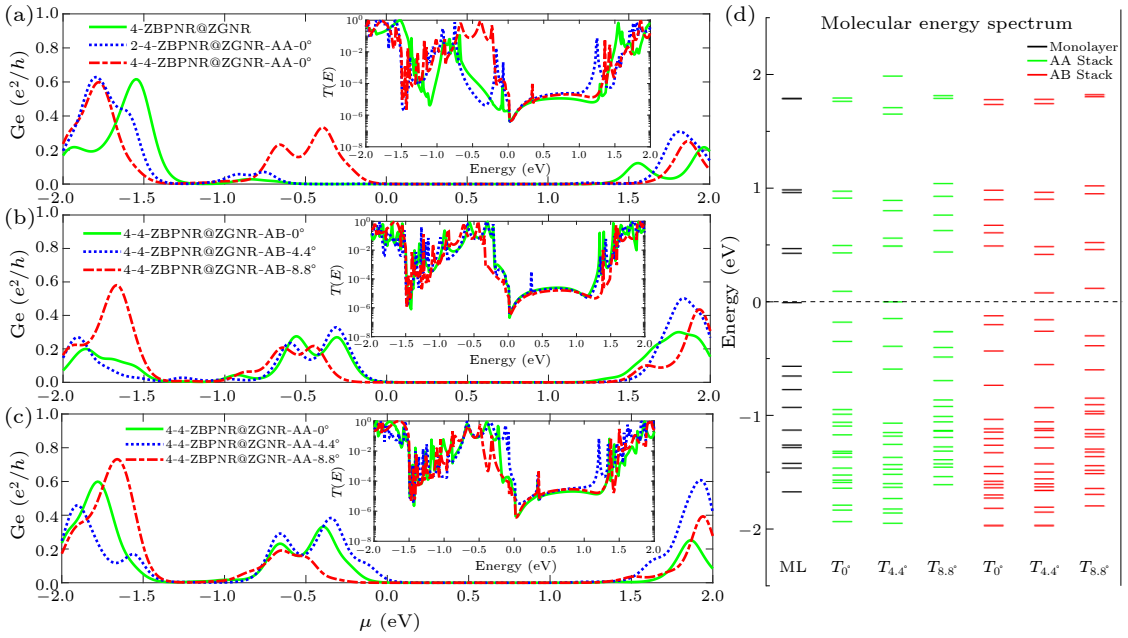

Fig. 3. The electrical conductance as a function of electrochemical potential μ at temperature $T = 500$ K for different configurations. (a) 4-ZBPNR@ZGNR, 2-4-ZBPNR@ZGNR-AA-0°, and 4-4-ZBPNR@ZGNR-AA-0°. (b) 4-4-ZBPNR@ZGNR-AB-0°, 4-4-ZBPNR@ZGNR-AB-4.4°, and 4-4-ZBPNR@ZGNR-AB-8.8°. (c) 4-4-ZBPNR@ZGNR-AA-0°, 4-4-ZBPNR@ZGNR-AA-4.4°, and 4-4-ZBPNR@ZGNR-AA-8.8°. (d) The corresponding molecular energy spectra.

a result, the transmission and electrical conductance peaks are also far away from the FL, as shown in Fig. 3(b). Especially, the added transport channels in the stacked layer can induce more severe fluctuations in electron transport. These more severe fluctuations of electronic transmissions can strongly enhance the Seebeck coefficient and power factor.

To elucidate these results, we calculate the local density of states (LDOS) of 4-ZBPNR@ZGNR, 4-4-ZBPNR@ZGNR-AA-0°, 4-4-ZBPNR@ZGNR-AA-4.4°, and 4-4-ZBPNR@ZGNR-AB-8.8° at different energies. In Fig. 4(a), the distribution of LDOS approaches zero in the ZBPNR of 4-ZBPNR@ZGNR at energy −0.23 eV, which means that the wave functions of the left electrode cannot match with those of the right electrode, leading to a very low electrical transmission coefficient. While for 4-4-ZBPNR@ZGNR-AA-0° in Fig. 4(b), although the distributions of LDOS in the top and bottom ZBPNRs are both nonuniform, the LDOS shows a mixed characteristic, meaning that the LDOS over the top and bottom ZBPNRs both participate in the carrier transport and the fusing between the layers forms a delocalization of electron density. Thus, the wave functions overlap in the top and bottom ZBPNRs, permitting carrier injection from the right electrode to the double-layer stacking ZBPNR and finally to the left electrode, forming new transport channels in the 4-4-ZBPNR@ZGNR-AA-0°. As a result, the electrical transmission coefficient of 4-4-ZBPNR@ZGNR-AA-0° is much larger than that of 4-ZBPNR@ZGNR at −0.23 eV. Compared to the LDOS at −0.12 eV with that at −0.23 eV, a striking difference is that the LDOS of the 4-4-ZBPNR@ZGNR-AA-0° at the center bilayer stacking ZBPNR region is almost disappeared, and the wave functions of the right electrode cannot touch those of the left electrode due to the absence of LDOS in the 4-4-ZBPNR@ZGNR-AA-0°. As a result, the transmission coefficients of the 4-4-ZBPNR@ZGNR-AA-0° significantly decrease. When varying the twist angle from 0° to 4.4°, the LDOS for 4-4-ZBPNR@ZGNR-AA-4.4° distributes over the whole central bilayer stacking ZBPNR, and the distributions of LDOS in the two ZBPNR layers are tightly entangled, implying strong interlayer interaction, as can be seen from Fig. 4(d). This strong interlayer interaction induces the electron from the right electrode can cross favourably the scattering region to the left electrode, which gives rise to rather large electron transmission coefficient, as shown in Fig. 3(c). However, it is clearly seen from Figs. 4(e) and 4(f) that when increasing the twist angle from 4.4° to 8.8°, the tightly entangled LDOS clearly disappears in the scattering region of the layer stack, which means that the transport channel of electrons in 4-4-ZBPNR@ZGNR-AB-8.8° is closed, resulting in a very low electron transmission coefficient. These results further reveal that the thermoelectricity in twisted bilayer BPNRHJ is very sensitive to the layer stacking and twist, which coincides well with previous result.[16]

To further understand the thermoelectric properties of the investigated devices, we study the influence of M-N-ZBPNR@ZGNR-AA-θ and M-N-ZBPNR@ZGNR-AB-θ with different twisting angles on the Seebeck coefficient S and power factor (PF) in Fig. 5. For 2-4-ZBPNR@ZGNR-AA-0° with ZBPNR stacking, the Seebeck coefficients are much higher than those in 4-ZBPNR@ZGNR within the energy region −0.5∼0.2 eV, where the top ZBPNR stacking plays the important role to in enhancing the Seebeck coefficient. This is because the stacked ZBPNR provides more electron transport pathways, and the oscillation of electrons in more electronic channels leads to more severe oscillations of the total electron transmission coefficient, hence resulting in much higher Seebeck coefficients.[67] Especially, our calculation shows that the Seebeck coefficients also depend on the stacking ZBPNR length, and the Seebeck coefficient peak in 4-4-ZBPNR@ZGNR-AA-0° is further enhanced compared with that of the 2-4-ZBPNR@ZGNR-AA-0° near the FL. In other words,

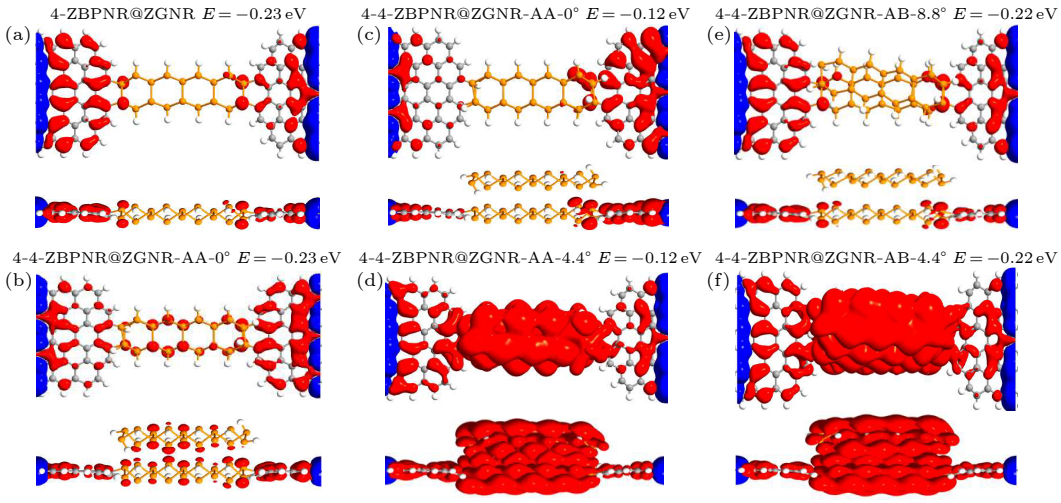

Fig. 4. The LDOS of (a) 4-ZBPNR@ZGNR at −0.23 eV, (b) 4-4-ZBPNR@ZGNR-AA-0° at −0.23 eV, (c) 4-4-ZBPNR@ZGNR-AA-0° at −0.12 eV, (d) 4-4-ZBPNR@ZGNR-AA-4.4° at −0.12 eV, (e) 4-4-ZBPNR@ZGNR-AB-8.8° at −0.22 eV, and (f) 4-4-ZBPNR@ZGNR-AB-4.4° at −0.22 eV, respectively.

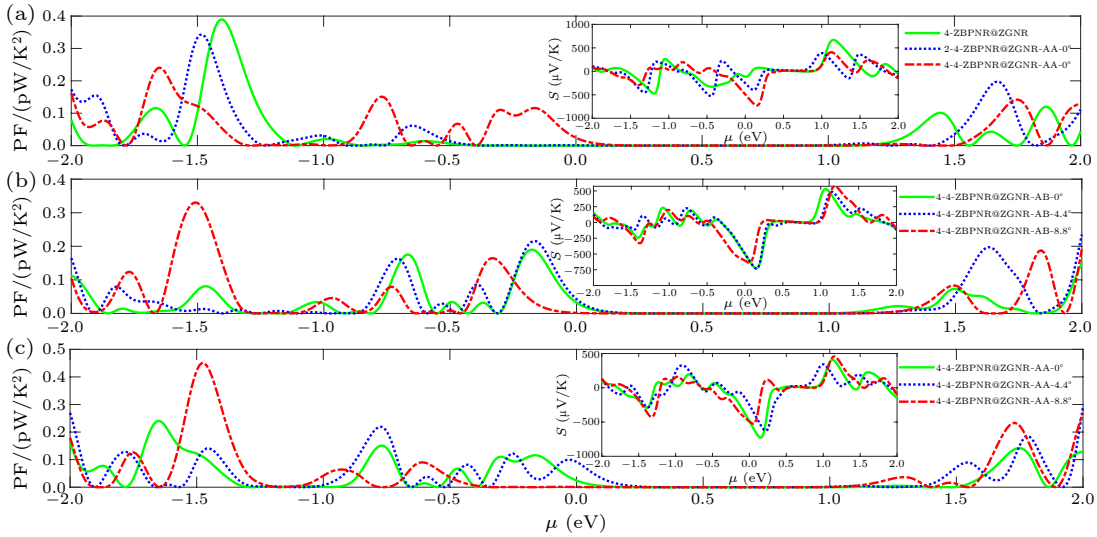

Fig. 5. The power factor (PF) as a function of electrochemical potential μ at temperature $T = 500\,\mathrm{K}$ for different configurations. (a) 4-ZBPNR@ZGNR, 2-4-ZBPNR@ZGNR-AA-0°, and 4-4-ZBPNR@ZGNR-AA-0°. (b) 4-4-ZBPNR@ZGNR-AB-0°, 4-4-ZBPNR@ZGNR-AB-4.4°, and 4-4-ZBPNR@ZGNR-AB-8.8°. (c) 4-4-ZBPNR@ZGNR-AA-0°, 4-4-ZBPNR@ZGNR-AA-4.4°, and 4-4-ZBPNR@ZGNR-AA-8.8°. The inserts describe the corresponding Seebeck coefficient S.

a longer layered stacking is beneficial for enhancing the Seebeck coefficient in bilayer stacking BPNRHJ. Combining this with very large electrical conductances within this energy region, significantly improved power factors can be obtained in 4-4-ZBPNR@ZGNR-AA-0°. When the twist angle is increased from 0° to 4.4° and then to 8.8°, the Seebeck coefficient curves also present an obvious twist-angle dependence. This can be mainly attributed to the twist-angle-dependent electron transmission curve (see Fig. 3). Simultaneously taking into account the angle modulation on electrical conductance, the calculations show that the power factor peaks in 4-4-ZBPNR@ZGNR-AA-θ and 4-4-ZBPNR@ZGNR-AB-θ can be significantly modulated by the twisting angle. Especially at $\mu = -1.4\,\mathrm{eV}$, a violent fluctuation of electronic transmission induces a very high Seebeck coefficient ($S = 500\,\mu\mathrm{V/K}$) in 4-4-ZBPNR@ZGNR-AA-8.8°. At the same time, a large electrical conductance exists at this energy position. These two combined factors result in the optimal PF in 4-4-ZBPNR@ZGNR-AA-8.8°. Compared with the AA stack, the AB stack can significantly improve the PF near the FL [see Fig. 5(b)]. Considering all these effects, our calculation shows that the bilayer stacking BPNRHJ with different twisting angles can not only improve the PF but also efficiently tune their chemical potential position.

Finally, we study the dependence of thermal conductance properties on twist angle θ. It is well known that thermal conductances are mainly contributed by electrons and phonons, and a low thermal conductance is required in thermoelectric devices to achieve high performance. Clearly from the insert in Fig. 6(a), relative to 4-ZBPNR@ZGNR, the phonon thermal conductances in bilayer stacking BPNRHJs are slightly increased. This increase in phonon thermal conductance is mainly attributed to the phonon interference between the layers. Varying the twist angle θ between the bilayer ZBPNR, the twist angle can serve as an independent degree of freedom to effectively induce and quantitatively modulate the phonon interference,[33] which can change the phonon thermal conductance. This regulation is also closely related to the configuration of the upper ZBPNR and can be confirmed by the results shown in the inserts in Figs. 6(b) and 6(c). Compared with the very small regulation by the stack and the twist on phonon thermal conductance, the electronic thermal conductance can be significantly modulated by these two factors, which is due to the stronger layer stack and twist dependence of the electrical conductance (see Fig. 3). This indicates that the regulation of the layer stack and twist on thermal conductance is mainly on electronic thermal conductance rather than on phonon thermal conductance. Clearly shown in Figs. 5(a) and 6(a), although the PF and thermal conductance in 4-4-ZBPNR@ZGNR-AA-0° are the largest compared with those in 4-ZBPNR@ZGNR and 2-4-ZBPNR@ZGNR-AA-0° at $\mu = -0.2\,\mathrm{eV}$, the PF will win the competition with the thermal conductance. Thus the $ZT_{\max}$ in 4-4-ZBPNR@ZGNR-AA-0° also reaches the largest value of 0.8. However, near the FL, the power factor peak of 4-4-ZBPNR@ZGNR-AB-4.4° is much larger than that of 4-4-ZBPNR@ZGNR-AA-4.4°, while the thermal conductance presents the opposite result, resulting in a much higher $ZT_{\max} = 1.4$ at $\mu = -0.14\,\mathrm{eV}$. Especially, although the PF increases significantly with the twist angle θ increasing from 0° to 8.8° at $\mu = -1.4\,\mathrm{eV}$ in 4-4-ZBPNR@ZGNR-AA-8.8°, the electronic thermal conductance has hardly changed, which leads to the optimal $ZT_{\max} = 2.5$ in 4-4-ZBPNR@ZGNR-AA-8.8°. These results indicate that the layer stack and interlayer twist can significantly regulate the thermoelectricity ZT.

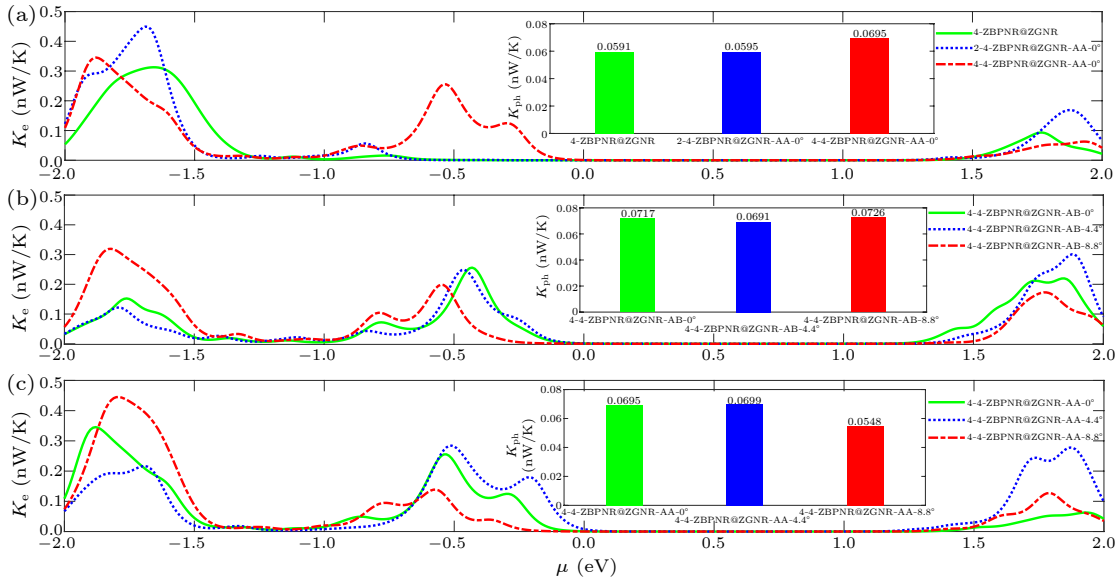

Fig. 6. (a)–(c) The electrical thermal conductance as a function of electrochemical potential μ at temperature $T = 500$ K for different configurations. (a) 4-ZBPNR@ZGNR, 2-4-ZBPNR@ZGNR-AA-0°, and 4-4-ZBPNR@ZGNR-AA-0°. (b) 4-4-ZBPNR@ZGNR-AB-0°, 4-4-ZBPNR@ZGNR-AB-4.4°, and 4-4-ZBPNR@ZGNR-AB-8.8°. (c) 4-4-ZBPNR@ZGNR-AA-0°, 4-4-ZBPNR@ZGNR-AA-4.4°, and 4-4-ZBPNR@ZGNR-AA-8.8°. The inserts describe the corresponding phonon thermal conductance at temperature $T = 500$ K.

4. Conclusion. In summary, we systematically study the electronic and thermoelectric performance in twisted bilayer BPNRHJ by using a combination of density functional theory and nonequilibrium Green's function method. Compared with the thermoelectric performance in BPNRHJ without BPNR stack, the thermoelectric performance can be improved significantly in BPNRHJ with BPNR stack due to the provided transport channels in stacked BPNR. Moreover, the twist angle can modulate the coupling strength of the Coulomb interaction between the layers, which induces severe fluctuations in electronic transport and hence enhances PF. While the phonon thermal conductance is almost insensitive to the layer stack and twist, the regulation by layered stack and twist on thermal conductance is mainly on electronic thermal conductance rather than on phonon thermal conductance. As a consequence, the figure of merit will be over 2.5 in 4-4-ZBPNR@ZGNR-AA-8.8°. Our results confirm that layer stack and twist are useful degrees of freedom to control the thermoelectric properties and will be helpful for the design and fabrication of a new generation of high-performance thermoelectric devices.

Acknowledgements. This work was supported by the Key Projects of Department of Education of Hunan Province, China (Grant No. 21A0167), the Natural Science Foundation of Hunan Province, China (Grant No. 2019JJ40532), and the Talent Introducing Foundation of Central South University of Forestry and Technology (Grant No. 104-0160).

References

[1] Hu J, Rigosi A F, Newell D B, and Chen Y P 2020 *Phys. Rev. B* **102** 235304
[2] Koshino M and Nam N N T 2020 *Phys. Rev. B* **101** 195425
[3] Ochoa H 2019 *Phys. Rev. B* **100** 155426
[4] Eliel G S N, Moutinho M V O, Gadelha A C, Righi A, Campos L C, Ribeiro H B, and Pimenta M A 2018 *Nat. Commun.* **9** 1221
[5] Wu K, Rademaker L, and Zaanen J 2014 *Phys. Rev. Appl.* **2** 054013
[6] Wang R, Chang K, Duan W H, Xu Y, and Tang P Z 2025 *Phys. Rev. Lett.* **134** 026904
[7] Gadelha A C, Ohlberg D A, Rabelo C, Neto E G, Vasconcelos E G, Campos J L, and Jorio A 2021 *Nature* **590** 405
[8] Cao Y, Fatemi V, Fang S, Watanabe K, Taniguchi T, Kaxiras E, and Jarillo-Herrero P 2018 *Nature* **556** 43
[9] Po H C, Zou L, Vishwanath A, and Senthil T 2018 *Phys. Rev. X* **8** 031089
[10] Yankowitz M, Chen S, Polshyn H, Zhang Y, Watanabe K, Taniguchi T, and Dean C R 2019 *Science* **363** 1059
[11] Chi H and Moodera J S 2022 *APL Mater.* **10** 090903
[12] Li Z, Zhuang C J, Chen L, Ni Z Y, Liu C, Wang L, Xu X, Wang J O, Pi X D, Wang X L, Du Yi, Wu K H, and Dou S X 2016 *ACS Cent. Sci.* **2** 517
[13] Suri N, Wang C, Zhang Y, and Xiao D 2021 *Nano Lett.* **21** 10026
[14] Zhu H, Yi J, Li M Y, Xiao J, Zhang L, Yang C W, and Zhang X 2018 *Science* **359** 579
[15] Mahapatra P S, Mahapatra K, Krishnamurthy H R, Mukerjee S, and Ghosh A 2017 *Nano Lett.* **17** 6822
[16] Mahapatra P S, Ghawri B, Garg M, Mandal S, Watanabe K, Taniguchi T, and Ghosh A 2020 *Phys. Rev. Lett.* **125** 226802
[17] Duan S, Cui Y, Yi W, Chen X, Yang B, and Liu X 2022 *Small* **18** 2204197
[18] Shi X L, Zou J, and Chen Z G 2020 *Chem. Rev.* **120** 7399
[19] Watts M C, Chen M C, Picco L, Russell-Pavier F S, Cullen P L, Miller T S, Bartuś S P, and Howard C A 2019 *Nature* **568** 216
[20] Li L, Yu Y, Ye G J, Ge Q, Qu X, Wu H, and Zhang Y 2014 *Nat. Nanotech.* **9** 372
[21] Liu H, Neal A T, Zhu Z, Luo Z, Liu H, Neal A T, Zhu Z, Zhu Z, Xu X, Tománek D, and Ye P D 2014 *ACS Nano* **8** 4033

[22] Ding Z K, Zeng Y J, Liu W, Tang L M, and Chen K Q 2024 *Adv. Funct. Mater.* **34** 2401684
[23] Tang X, Zhang K B, Tang S H, Peng X F, and Long M Q 2025 *Chem. Phys.* **591** 112585
[24] Li Z Y, Qian H Y, Wu J, and W Duan 2008 *Phys. Rev. Lett.* **100** 206802
[25] Ding Z K, Zeng Y J, Pan H, Luo N N, Tang L M, Zeng J, and Chen K Q 2024 *Phys. Rev. B* **109** 245104
[26] Brandimarte P, Engelund M, Papior N, Garcia-Lekue A, Frederiksen T, and Sánchez-Portal D 2017 *J. Chem. Phys.* **146** 092318
[27] Ouyang T, Chen Y P, Xie Y, Wei X L, Yang K, Yang P, and Zhong J 2010 *Phys. Rev. B* **82** 245403
[28] Xu Y, Chen X B , Wang J S, Gu B L, and Duan W H 2010 *Phys. Rev. B* **81** 195425
[29] Liu W, Z K Ding, N Luo, J Zeng, Tang L M, and Chen K Q 2024 *Phys. Rev. B* **109** 115422
[30] Wu D, Huang L, Jia P Z, Cao X H, Fan Z Q, Zhou W X, and Chen K Q 2021 *Appl. Phys. Lett.* **119** 063503
[31] Wang D, Bao D, Zheng Q, Wang C T, Wang S, Fan P, and Gao H J 2023 *Nature Commun.* **14** 1018
[32] Sanz S, Papior N, Giedke G, Sánchez-Portal D, Brandbyge M, and Frederiksen T 2022 *Phys. Rev. Lett.* **129** 037701
[33] Zeng Y J, Wu D, Cao X H, Feng Y X, Tang L M, and Chen K Q 2020 *J. Mater. Chem. A* **8** 11884
[34] Liu W P, Ding Z K, Luo N N, Zeng J, Tang L M, and Chen K Q 2025 *Phys. Rev. B* **111** 115407
[35] Ostovan A, Milowska K Z, and García-Cervera C J 2024 *Nanoscale* **16** 7504
[36] Kim K, Yankowitz M, Fallahazad B, Kang S, Movva H C P, Huang S Q, Larentis S, Corbet C M, Taniguchi T S, and Watanabe K J 2016 *Nano Lett.* **16** 1989
[37] Ribeiro-Palau R, Zhang C, Watanabe K, Taniguchi T, Hone J, and Dean C R 2018 *Science* **361** 690
[38] Pishevar E and Karamitaheri H 2024 *Adv. Theory Simul.* **7** 2301082
[39] Guan J, Zhu Z, and Tománek D 2014 *Phys. Rev. Lett.* **113** 046804
[40] Wu M, Fu H, Zhou L, Yao K, and Zeng X C 2015 *Nano Lett.* **15** 3557
[41] Shi H L, Yang J, Han Q Z, Wang C Z, Zhong S, Sun S, and Chen W 2016 *Nano Lett.* **16** 4903
[42] Zhu Z and Tománek D 2014 *Phys. Rev Lett.* **112** 176802
[43] Aierkenl Y, Cakirl D, and Sevik C 2015 *Phys. Rev. B* **92** 081408
[44] Sevik C and Sevinçli H 2016 *Nanotechnology* **27** 355705
[45] Hu R, Zhou Z Z, and Sheng C Y 2020 *Phys. Chem. Chem. Phys.* **22** 22390
[46] Sun M, Tang W, Li S, Chou J P, Hu A, and Schwingenschlögl U 2020 *J. Phys. Condens. Matter* **32** 055501
[47] Zhu S C, Peng S J, Wu K M, Yip C T, Yao K L, and Lam C H 2018 *Phys. Chem. Chem. Phys.* **20** 21105
[48] Zhu L, Li B, and Yao K 2018 *Nanotechnology* **29** 325206
[49] Shi H L, Yang J, Han Q Z, Ren Y H, Zhao Y H, He S Y, and Jiang Z T 2023 *Nanotechnology* **34** 375703
[50] Sodagar S, Karbaschi H, Soltani M, and Amini M 2022 *Physica Scripta* **98** 015001
[51] Zhu H 2021 *Phys. B* **605** 412774
[52] Rezaei M, Karbaschi H, Amini M, Soltani M, and Rashedi G 2021 *Nanotechnology* **32** 375704
[53] Taylor J, Guo H, and Wang J 2001 *Phys. Rev. B* **63** 245407
[54] Brandbygel M, Mozos J, Ordejón P, Taylor J, and Stokbro K 2002 *Phys. Rev. B.* **65** 165401
[55] Wu D, Cao X H, Jia P Z, Zeng Y J, Feng Y X, Tang L M, and Chen K Q 2020 *Sci. China Phys. Mech. Astron.* **63** 276811
[56] Wang J S, Wang J, and Lü J T 2008 *Eur. Phys. J. B* **62** 381
[57] Jiang J W, Wang J S, and Li B W 2011 *J. Appl. Phys.* **109** 014326
[58] Dey U and Chattopadhyay A 2025 *Adv. Quantum Technol.* 2400569
[59] Chen C C, Li Z, Shi L, and Cronin S B 2015 *Nano Research.* **8** 666
[60] Cahill D G 2005 *Rev. Sci. Instrum.* **75** 5119
[61] Liu Z, Morales-Ferreiro J O, and Luo T 2018 *Appl. Phys. Lett.* **113** 063903
[62] Cao X H, Wu D, Peng Y X, Zhou W X, Tang L M, and Chen K Q 2019 *J. Phys.: Condens. Matter* **31** 345303
[63] Zhang K B, Tan S H, Peng X F, and Long Q M 2024 *Chin Phys. Lett.* **41** 097301
[64] Ma L, Nian L L, and Lü J T 2020 *Phys. Rev. B* **101** 045410
[65] Huang L F, Zhou Y, Chen Y R, Ye J Y, Liu J Y, Xiao Z Y,Tang C, Xia H P, and Hong W J 2021 *Sci. China Chem.* **64** 1426
[66] Garner M H, Li H, Chen Y, Su A, Shangguan Z, Paley D W, and Solomon G C 2018 *Nature* **558** 415
[67] Gunst T, Markussen T, Jauho A P, and Brandbyge M 2011 *Phys. Rev. B* **84** 155449